Available online at www.sciencedirect.com
SCIENCE DIRECT®
Journal of Applied Geophysics 54 (2003) 297–318
JOURNAL OF APPLIED GEOPHYSICS
www.elsevier.com/locate/jappgeo

Converted-wave moveout and conversion-point equations in layered VTI media: theory and applications

Xiang-Yang Li[a,*], Jianxin Yuan[b]

[a] British Geological Survey, West Mains Road, Edinburgh EH9 3LA, Scotland, UK
[b] PGS Inc., 10550 Richmond Avenue, Suite 300, Houston, TX 77042, USA

Abstract

We have developed improved equations for calculating the conversion point of the P-SV converted wave (C-wave) in transversely isotropic media with a vertical symmetry axis (vertical transverse isotropy (VTI)). We have also derived modified C-wave moveout equations for layered VTI media. The derived equations for the conversion-point are valid for offsets about three-times the reflector depth ($x/z = 3.0$) and those for the C-wave moveout about twice the reflector depth ($x/z = 2.0$). The new equations reveal some additional analytical insights into the converted-wave properties. The anisotropy has a more significant effect on the conversion point than on the moveout, and using the effective binning velocity ratio γ_{eff} only is often insufficient to account for the anisotropic effect, even when higher-order terms are considered. Also for C-wave propagation, the anisotropy appears to affect the P-wave leg more than the S-wave leg. The ratio of the anisotropic contributions from P- and S-waves is close to the vertical velocity ratio γ_0. Consequently S-wave anisotropic parameters may be recovered from converted-waves when P-wave anisotropic parameters are known. The new equations suggest that the C-wave moveout in layered VTI media over intermediate-to-far offsets is determined by the anisotropic parameter χ_{eff} in addition to C-wave stacking velocity V_{C2}, and the velocity ratios γ_0 and γ_{eff}. We refer to these four parameters as the C-wave "stacking velocity model". Two practical work flows are presented for determining this model: the double-scanning flow and the single-scanning flow. Applications to synthetic and real data show that although the single-scanning flow is less accurate than the double-scanning flow, it is more efficient and, in most cases, can yield sufficiently accurate results.

Keywords: Converted-waves; Transverse isotropy; Parameter estimation; VTI

1. Introduction

Converted-wave (C-wave) moveout is inherently non-hyperbolic and has been intensively studied over recent years (e.g. Tsvankin and Thomsen, 1994; Li and Yuan, 1999; Cheret et al., 2000; Tsvankin and Grechka, 2000a,b; Tsvankin, 2001). Apart from the asymmetric raypath, the wide occurrence of polar anisotropy (vertical transverse isotropy, VTI) in marine sediments and the associated layering effects contribute to the non-hyperbolic behaviour. One common approach in describing the non-hyperbolic moveout is the use of a higher-order Taylor series expansion. This approach is good for parameter estimation and makes it possible to process C-wave data independently of P-waves. Thomsen (1999) gave a good description of the Taylor-series ap-

* Corresponding author. Tel.: +44-131-667-1000; fax: +44-131-667-1877.
E-mail address: xyl@bgs.ac.uk (X.-Y. Li).

0926-9851/$ - see front matter © 2003 Elsevier B.V. All rights reserved.
doi:10.1016/j.jappgeo.2003.02.001

proach, which was widely used in the industry. However, the equations of Thomsen (1999) for the moveout are limited to the middle offsets approximately equal to the reflector depth (offset-depth ratio $x/z = 1.0$). Note that, for reaction moveout, Thomsen (1999) presented a simplified version of the equations given in Tsvankin and Thomsen (1994), which is accurate up to offsets about twice the reflector depth ($x/z = 2.0$).

In addition to moveout analysis, determining the conversion point is also an important step in C-wave processing. Traditionally, there are also two approaches to this problem. One approach involves solving a fourth order polynomial equation, (e.g. Tessmer and Behle, 1988), and the other is based on the Taylor series expansion of the conversion-point offset, including both asymptotic (first-order) and higher-order expansions (e.g. Thomsen, 1999). However, most of these equations have been derived only for layered isotropic media.

The above shortcomings of the existing theory have limited the use of anisotropy in C-wave processing. When the need for anisotropic processing arises, ray-tracing has been the main tool for calculating C-wave travel-times. Ray tracing itself is very accurate, but there is a lack of effective tools to build the anisotropic model for ray tracing purposes. Existing methods for model building are often based on borehole extrapolation. This substantially increases the turnaround time, and the result may also not be sufficiently accurate for areas away from the borehole. Thus more accurate analytical theories are required to understand the converted-wave behaviour and to simplify the processing sequence.

Recently, 4C seismic acquisition has become increasingly common in the industry due to the potential for imaging through gas clouds and lithology-fluid prediction. For analyzing the reaction moveout in 4C seismic data, various velocities, velocity ratios and anisotropic parameters have been used in the literature. For example, there are stacking velocities for P-, S- and C-waves, V_{P2}, V_{S2} and V_{C2}, respectively, vertical and effective binning velocity ratios γ_0 and γ_{eff}, and anisotropic parameters η and σ, etc. The key issue is how to retrieve these parameters robustly from 4C data and build an accurate anisotropic velocity model.

Gaiser and Jackson (2000) and Thomsen (1999) proposed the following procedures to estimate some of those parameters: determine V_{C2} from short-spread hyperbolic moveout analysis, γ_0 from a coarse correlation of P- and C-wave stacked sections, and invert γ_{eff} from V_{C2} and the P-wave short-spread stacking velocity V_{P2}. However, there are often 3–5% errors associated with C-wave short-spread stacking velocities, and this error increases with offsets. This may not be a serious problem for P-wave processing, but it is very critical for C-waves, due to severe error propagation. Existing results in P-wave data analysis (Grechka and Tsvankin, 1988) suggest that it may be possible to determine V_{C2} accurately using a generic non-hyperbolic moveout equation with fitted coefficients. This idea will be utilized for building new work flows for processing 4C seismic data.

In this paper, we first introduce the notation and present improved equations for calculating the C-wave conversion point in layered VTI media. We then present the modified moveout equation and discuss its implications for parameter estimation. Following that, we present two work flows for determining the C-wave stacking velocity model. illustrated by both synthetic and real data examples.

2. Notation and definitions

Throughout the paper, Thomsen's (1999) notation is used. Subscripts P, S and C denote P-, S- and C-waves, respectively. Subscript 1 denotes interval quantities, subscript 2 denotes root-mean-squared (rms) quantities and subscript 0 denotes vertical, or average quantities where appropriate. t stands for travel time. V for velocity and γ for velocity ratio. Thus, t_{P0}, t_{S0} and t_{C0} stand for the vertical travel-time for P-, S- and C-wave, respectively; V_{P0}, V_{S0} and V_{C0} stand for the vertical or average velocities for the three waves, respectively; V_{P2}, V_{S2} and V_{C2} stand for the stacking (rms) velocities; γ_0, γ_2 and γ_{eff} stand for the vertical, stacking (rms) and effective velocity ratios, respectively.

2.1. Model and definitions

Consider an n-layered VTI medium, and a P-SV wave converted at the bottom of the n-th layer with a

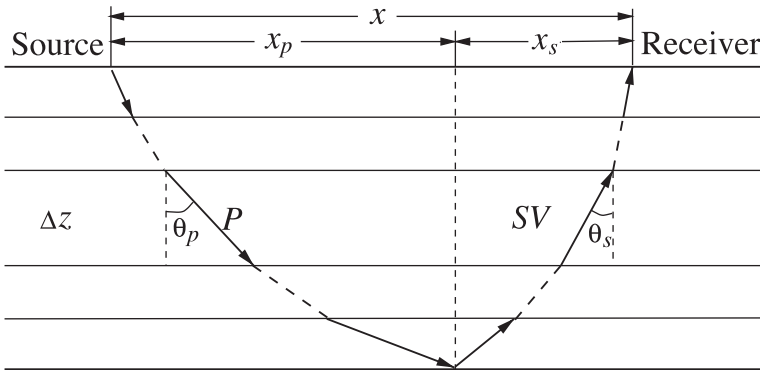

Fig. 1. Geometry of converted-wave raypath in horizontally layered transversely isotropic media.

down-going P-wave leg and an up-going SV-wave leg (Fig. 1). Each layer in the model is homogeneous with the following interval parameters for the i-th layer ($i=1,2,\ldots,n$): P- and S-wave vertical velocities V_{P0i} and V_{S0i}, P- and S-wave short-spread NMO velocities V_{P2i} and V_{S2i}, vertical one-way travel times Δt_{P0i} and Δt_{S0i}, respectively, and Thomsen (1986) parameters ϵ_i and δ_i.

Using Thomsen's (1999) notation, the velocity ratios are defined as

$$\gamma_{0i}=\frac{V_{P0i}}{V_{S0i}};\quad \gamma_{2i}=\frac{V_{P2i}}{V_{S2i}};\quad \gamma_{\mathrm{eff}i}=\frac{\gamma_{2i}^2}{\gamma_{0i}} \tag{1}$$

and the interval parameters and rms quantities have the following relationship,

$$t_{P0}=\sum_{i=1}^{n}\Delta t_{P0i};\quad t_{S0}=\sum_{i=1}^{n}\Delta t_{S0i};\quad t_{C0}=t_{P0}+t_{S0}, \tag{2}$$

$$V_{P2}^2=\frac{1}{t_{P0}}\sum_{i=1}^{n}V_{P2i}^2\Delta t_{P0i};\quad V_{S2}^2=\frac{1}{t_{S0}}\sum_{i=1}^{n}V_{S2i}^2\Delta t_{S0i}, \tag{3}$$

$$t_{C0}V_{C2}^2=t_{P0}V_{P2}^2+t_{S0}V_{S2}^2, \tag{4}$$

and

$$\gamma_0=\frac{t_{S0}}{t_{P0}};\quad \gamma_2=\frac{V_{P2}}{V_{S2}};\quad \gamma_{\mathrm{eff}}=\frac{\gamma_2^2}{\gamma_0}. \tag{5}$$

2.2. Basic relationships

From the above definitions, we can derive the following relationships between the velocity ratios and stacking velocities,

$$\gamma_{\mathrm{eff}}=\frac{V_{P2}^2}{V_{C2}^2(1+\gamma_0)-V_{P2}^2}, \tag{6}$$

$$V_{P2}^2=V_{C2}^2\frac{\gamma_{\mathrm{eff}}(1+\gamma_0)}{1+\gamma_{\mathrm{eff}}}, \tag{7}$$

and

$$V_{S2}^2=V_{C2}^2\frac{1+\gamma_0}{(1+\gamma_{\mathrm{eff}})\gamma_0}. \tag{8}$$

2.3. Anisotropic parameters η and ζ

Introduce two more anisotropic parameters η_i and ζ_i satisfying

$$\eta_i=\frac{(\epsilon_i-\delta_i)}{(1+2\delta_i)^2}\left(1+\frac{2\delta_i}{1-V_{S0i}^2/V_{P0i}^2}\right); \tag{9}$$

$$\zeta_i=\frac{\sigma_i}{(1+2\sigma_i)^2}\left(1+\frac{2\delta_i}{1-V_{S0i}^2/V_{P0i}^2}\right), \tag{10}$$

where σ_i is defined as

$$\sigma_i=\gamma_0^2(\epsilon_i-\delta_i). \tag{11}$$

The reason for introducing parameters η_i and ζ_i is that η_i controls the anisotropic behaviour in long-spread P-wave reaction moveout, and ζ_i controls the anisotropic

behaviour in intermediate-spread S-wave moveout, as shown by Tsvankin and Thomsen (1994). Note that η_i in Eq. (9) is different from the conventional definition, which it will reduce to after some simplifications (see below). η_i and ζ_i also control the anisotropy in the calculation of the C-wave conversion point, as shown in Appendix A.

Eqs. (9) and (10) are the exact definitions and appear to be complicated in terms of practical applications. Alkhalifah and Tsvankin (1995) found that the effects of the term V_{S0i}/V_{P0i} in Eq. (9) is small and may be ignored for long-spread P-wave propagation. Similarly, Yuan (2002) found out that this term in Eq. (10) may also be neglected for intermediate-spread S-wave propagation. This leads to the following simplified expressions:

$$\eta_i = \frac{\epsilon_i - \delta_i}{1 + 2\delta_i}; \quad \zeta_i = \gamma_{\mathrm{eff}i}^2 \eta_i. \tag{12}$$

Eq. (12) shows that η_i is reduced to the anisotropic parameter η (Alkhalifah and Tsvankin, 1995).

3. Calculating the conversion point

VTI is common in sedimentary rocks. Thomsen (1999) discussed various methods to account for the anisotropic effects using isotropic methods for conversion-point calculation, where the effects of anisotropy were only considered in the form of the effective velocity ratio γ_{eff} (γ_{eff} "compensation"). This approach may introduce significant conversion-point errors even for relatively weak anisotropy over modest offset ranges ($x/z = 1.0$) (Gaiser and Jackson, 2000). For a homogeneous VTI medium, Li and Yuan (1999) derived a higher-order Taylor-series equation with sufficient accuracy up to $x/z = 3.0$. Here we extend the results of Li and Yuan (1999) to multilayered media.

3.1. Generalized equations

The conversion-point offset x_C for a C-wave ray converted at the bottom of the n-th layer and emerging at offset x can be written as (Fig. 1),

$$x_C = x\left(c_0 + \frac{c_2 x^2}{1 + c_3 x^2}\right), \tag{13}$$

where $c_3 = c_2/(1 - c_0)$ (Thomsen, 1999). Note that the conversion point offset x_C is defined as the offset of the P-wave leg, x_P, i.e., $x_C = x_P$ (Fig. 1). Coefficients c_0 and c_2 are derived as (Appendix A),

$$c_0 = \frac{\sum_{i=1}^{n} V_{\mathrm{P2}i}^2 \Delta t_{\mathrm{P0}i}}{\sum_{i=1}^{n} V_{\mathrm{P2}i}^2 \Delta t_{\mathrm{P0}i} + \sum_{i=1}^{n} V_{\mathrm{S2}i}^2 \Delta t_{\mathrm{S0}i}}, \tag{14}$$

and

$$c_2 = \frac{\left[\sum_{i=1}^{n} V_{\mathrm{S2}i}^2 \Delta t_{\mathrm{S0}i}\right]\left[\sum_{i=1}^{n} V_{\mathrm{P2}i}^2 \Delta t_{\mathrm{P0}i}(1 + 8\eta_i)\right] - \left[\sum_{i=1}^{n} V_{\mathrm{P2}i}^2 \Delta t_{\mathrm{P0}i}\right]\left[\sum_{i=1}^{n} V_{\mathrm{S2}i}^2 \Delta t_{\mathrm{S0}i}(1 - 8\zeta_i)\right]}{2\left[\sum_{i=1}^{n} V_{\mathrm{P2}i}^2 \Delta t_{\mathrm{P0}i} + \sum_{i=1}^{n} V_{\mathrm{S2}i}^2 \Delta t_{\mathrm{S0}i}\right]^4} \tag{15}$$

Substituting Eqs. (2)–(5) into Eqs. (14) and (15), and introducing

$$\eta_{\mathrm{eff}} = \frac{1}{8 t_{\mathrm{P0}} V_{\mathrm{P2}}^4}\left[\sum_{i=1}^{n} V_{\mathrm{P2}i}^4 (1 + 8\eta_i)\Delta t_{\mathrm{P0}i} - t_{\mathrm{P0}} V_{\mathrm{P2}}^4\right], \tag{16}$$

and

$$\zeta_{\mathrm{eff}} = \frac{1}{8 t_{\mathrm{S0}} V_{\mathrm{S2}}^4}\left[t_{\mathrm{S0}} V_{\mathrm{S2}}^4 - \sum_{i=1}^{n} \Delta t_{\mathrm{S0}i} V_{\mathrm{S2}i}^4 (1 - 8\zeta_i)\right], \tag{17}$$

gives

$$c_0 = \frac{\gamma_{\mathrm{eff}}}{1 + \gamma_{\mathrm{eff}}}, \tag{18}$$

and

$$c_2 = \frac{\gamma_{\mathrm{eff}}(1 + \gamma_0)}{2 t_{\mathrm{C0}}^2 V_{\mathrm{C2}}^2 \gamma_0 (1 + \gamma_{\mathrm{eff}})^3} \times [\gamma_0 \gamma_{\mathrm{eff}} - 1 + 8(\eta_{\mathrm{eff}} \gamma_0 \gamma_{\mathrm{eff}} + \zeta_{\mathrm{eff}})]. \tag{19}$$

η_{eff} is the effective anisotropic parameter for P-wave in multilayered media and is the same as the η_{eff} introduced by Alkhalifah and Tsvankin (1995). ζ_{eff} is the corresponding parameter for SV-wave in layered VTI media. For a single-layered VTI medium, η_{eff} and ζ_{eff} reduce to η and ζ, respectively.

3.2. Special cases

Let's examine whether the above equations reduce to the isotropic case as studied by Thomsen (1999) and the single-layered anisotropic case by Li and Yuan (1999).

3.2.1. Isotropic case

For layered isotropic media, the parameters η_{eff} and ζ_{eff} become

$$\eta_{\text{eff}} = \frac{1}{8t_{\text{P0}}V_{\text{P2}}^4}\left(\sum_{i=1}^{n} V_{\text{P2}i}^4 \Delta t_{\text{P0}i} - t_{\text{P0}}V_{\text{P2}}^4\right), \tag{20}$$

and

$$\zeta_{\text{eff}} = \frac{1}{8t_{\text{S0}}V_{\text{S2}}^4}\left(t_{\text{S0}}V_{\text{S2}}^4 - \sum_{i=1}^{n} \Delta t_{\text{S0}i} v_{\text{S2}i}^4\right). \tag{21}$$

In this case, η_{eff} and ζ_{eff} control the residual layering effects on P- and S-waves, respectively. Ignoring these residual effects leads to,

$$c_2 = \frac{\gamma_{\text{eff}}(1+\gamma_0)(\gamma_0\gamma_{\text{eff}} - 1)}{2t_{\text{C0}}^2 V_{\text{C2}}^2 \gamma_0 (1+\gamma_{\text{eff}})^3}. \tag{22}$$

Eq. (22) has the same form as the expression given by Thomsen (1999).

3.2.2. Single-VTI layer case

Using Eq. (12) for single-layer case, Eq. (19) reduces to

$$c_2 = \frac{\gamma_{\text{eff}}(1+\gamma_0)}{2t_{\text{C0}}^2 V_{\text{C2}}^2 \gamma_0 (1+\gamma_{\text{eff}})^3} \times [\gamma_0\gamma_{\text{eff}} - 1 + 8(\gamma_0 + \gamma_{\text{eff}})\gamma_{\text{eff}}\eta]. \tag{23}$$

This has the same form as the expression given by Li and Yuan (1999). Thus, the new generalized equations for multilayered VTI media do reduce to known equations for special cases.

3.3. Numerical accuracy

The accuracy of Eqs. (13), (18) and (19) is tested here by numerical modelling. Table 1 shows the parameters of a three-layer model. Each layer has a thickness of 500 m. The conversion points calculated by the approximations are compared with the results of ray-tracing. Fig. 2a shows the comparisons of the anisotropic Eqs. (13), (18) and (19) with ray tracing, and Fig. 2b shows the comparison of the isotropic Eqs. (13), (18) and (22) with ray tracing. Note that the difference between Fig. 2a and b lies in the calculation of the coefficient c_2. Fig. 2a uses the anisotropic Eq. (19) and Fig. 2b uses the isotropic Eq. (22). For all three reflectors, the conversion point error is less than 0.5% for $x/z = 1.0$ and less than 1.5% for $x/z = 3.0$ when using the anisotropic Eq. (19) (Fig. 2a). However, if the anisotropy parameters η_{eff} and ζ_{eff} are ignored, the error increases to 5% for $x/z = 1.0$ and to more than 10% for $x/z = 3.0$ (Fig. 2b).

Table 1
Parameters for a three-layer model with VTI anisotropy

No.	Material	$V_{\text{P0}i}$	$V_{\text{S0}i}$	ε_i	δ_i	V_{C2}	η_{eff}	ζ_{eff}
1	Dog Creek shale	1875	826	0.225	0.100	1541	0.104	0.154
2	Limestone shale	3306	1819	0.134	0.000	2047	0.187	0.130
3	Taylor sandstone	3368	1829	0.110	−0.035	2264	0.187	0.119

The layer parameters are taken from Thomsen (1986).

3.4. Effects of η_{eff} and ζ_{eff}

For most earth models, one can expect that η_{eff} and ζ_{eff} have the same sign. Thus, the residual term $[8(\eta_{\text{eff}}\gamma_0\gamma_{\text{eff}} + \zeta_{\text{eff}})]$ in Eq. (19) may often be of the same order as the first term $(\gamma_0\gamma_{\text{eff}} - 1)$. This confirms Gaiser and Jackson's (2000) numerical analysis that compensating for γ_{eff} only, i.e., ignoring the term $[8(\eta_{\text{eff}}\gamma_0\gamma_{\text{eff}} + \zeta_{\text{eff}})]$ in Eq. (19) is not sufficient to account for anisotropy. They also found that an increase in ϵ or a decrease in δ increases the errors in x_{C}. This can be easily explained by Eq. (19) or Eq. (23), since either an increase in ϵ or a decrease in δ gives rise to an increase in η or ζ, and hence increases the errors in x_{C}.

It is also worth noting that the residual term after γ_{eff} compensation in Eq. (19) is determined by the anisotropic parameters η and ζ, rather than by δ and σ directly. (As δ does for P-wave, σ measures the relative difference between the S-wave stacking and vertical velocity; Thomsen, 1986.) As shown in Sec-

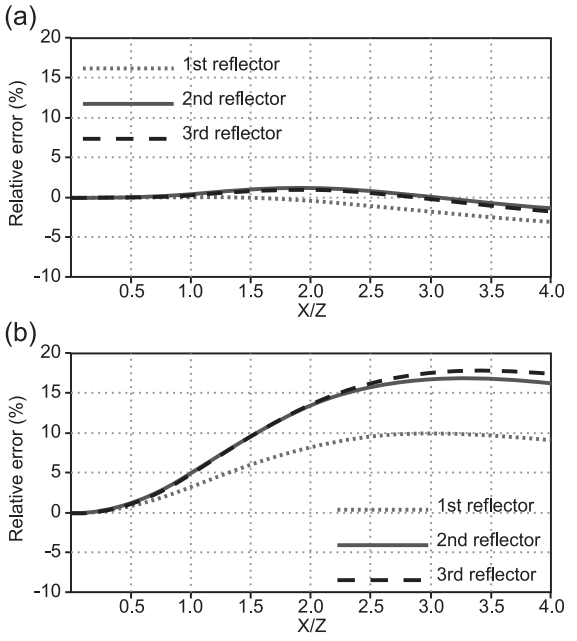

Fig. 2. Accuracy of approximations for the three-layer model in Table 1. (a) Results obtained from Eq. (19) that consider both γ_{eff} and the anisotropic residual term, and (b) results from Eq. (22) that only considers γ_{eff} and ignores the residual anisotropic term. The horizontal axis is the offset-to-depth ratio x/z, and the vertical axis is the relative error of the conversion point x_C calculated as $[x_C^{(\text{exact})} - x_C^{(\text{approx})}]/x$. The dotted line is from the first reflector, the solid line from the second reflector and the dashed line from the third reflector.

tion 4, C-wave moveout signature is also determined by η and ζ.

4. Taylor-series based moveout equations

Tsvankin and Thomsen (1994) derived a generic form of the C-wave moveout equation based on a Taylor series expansion, but their expression for the quadratic coefficient A_4 is of a complicate form. Thomsen (1999) and Cheret et al. (2000) presented simplified forms. However, the expression for A_4 in Thomsen's (1999) paper is less accurate and limited to an offset-depth ratio of 1.0. The expression for A_4 in Cheret et al. (2000) contains a parameter called the "horizontal converted-wave velocity" (V_{Ch}), which is not well defined and difficult to determine. Here, we present an alternative and more accurate approach to utilize the non-hyperbolic moveout equation of Tsvankin and Thomsen (1994) for moveout analysis in layered VTI media.

4.1. Generalized equations

The moveout for a C-wave ray t_C, converted at the bottom of the n-th layer and emerging at offset x (Fig. 1), can be written as (Tsvankin and Thomsen, 1994)

$$t_C^2 = t_{C0}^2 + \frac{x^2}{V_{C2}^2} + \frac{A_4 x^4}{1 + A_5 x^2} \tag{24}$$

where (see Appendix B)

$$A_4 = \frac{(\gamma_0\gamma_{\text{eff}} - 1)^2 + 8(1+\gamma_0)(\eta_{\text{eff}}\gamma_0\gamma_{\text{eff}}^2 - \zeta_{\text{eff}})}{4t_{C0}^2 V_{C2}^4 \gamma_0 (1+\gamma_{\text{eff}})^2}, \tag{25}$$

and

$$A_5 = \frac{A_4}{1/V_{\text{Ph}}^2 - 1/V_{C2}^2}. \tag{26}$$

V_{Ph} is the horizontal P-wave velocity.

4.2. The four-parameter moveout equation

Introduce a combined parameter χ_{eff},

$$\chi_{\text{eff}} = \eta_{\text{eff}}\gamma_0\gamma_{\text{eff}}^2 - \zeta_{\text{eff}}, \tag{27}$$

which describes the total influence of the VTI and layering on the C-wave moveout signature. Note that for a single VTI layer, Eq. (27) reduces to

$$\chi = \eta(\gamma_0 - 1)\gamma_{\text{eff}}^2. \tag{28}$$

substituting Eq. (27) into Eq. (25) gives

$$A_4 = -\frac{(\gamma_0\gamma_{\text{eff}} - 1)^2 + 8(1+\gamma_0)\chi_{\text{eff}}}{4t_{C0}^2 V_{C2}^4 \gamma_0 (1+\gamma_{\text{eff}})^2}. \tag{29}$$

Following Alkhalifah and Tsvankin's (1955) empirical relationship between V_{Ph} and η_{eff}, we suggest a similar empirical relationship between V_{Ph} and χ_{eff},

$$V_{\text{Ph}} = V_{\text{P2}}\sqrt{1+2\eta} \approx V_{\text{P2}}\sqrt{1 + \frac{2\chi_{\text{eff}}}{(\gamma_0 - 1)\gamma_{\text{eff}}^2}}. \tag{30}$$

The above equation is strictly valid only for a single VTI layer, but it is a good approximation for moveout analysis in layered media. Substituting Eqs. (29) and (30) into Eq. (26) and using Eq. (7) gives,

$$A_5 = \frac{A_4 V_{C2}^2 (1+\gamma_0)\gamma_{eff}\left[(\gamma_0-1)\gamma_{eff}^2 + 2\chi_{eff}\right]}{(\gamma_0-1)\gamma_{eff}^2(1-\gamma_0\gamma_{eff}) - 2(1+\gamma_0)\gamma_{eff}\chi_{eff}}. \tag{31}$$

Thus, the C-wave moveout, as described by Eqs. (24), (29) and (31), is controlled by four parameters, V_{C2}, γ_0, γ_{eff} and χ_{eff}. We refer to Eqs. (24), (29) and (31) as the four parameter equations, which form the basis for parameter estimation and moveout correction. Note that the *P*-wave moveout signature is controlled only by two parameters V_{P2} and η_{eff}.

4.3. Special cases

Here, for comparison, we consider the special cases of a single isotropic layer and a single VTI layer, which were studied by Thomsen (1999).

4.3.1. Single isotropic layer

In this case, $\gamma_{eff}=\gamma_0$, $\chi_{eff}=0$ and Eqs. (29) and (31) reduce to

$$A_4 = \frac{-(\gamma_0-1)^2}{4t_{C0}^2 V_{C2}^4 \gamma_0}; \quad A_5 = \frac{A_4 V_{C2}^2 \gamma_0}{1-\gamma_0}. \tag{32}$$

Eq. (32) differs from the original equation given in Thomsen (1999) here referred to as A_4^*, which has the following form,

$$A_4^* = \frac{-(\gamma_0-1)^2}{4t_{C0}^2 V_{C2}^4 (\gamma_0+1)}; \quad A_5 = \frac{A_4^* V_{C2}^2 \gamma_0}{1-\gamma_0}. \tag{33}$$

4.3.2. Single VTI layer

In this case, Eq. (29) reduces to

$$A_4 = \frac{-1}{t_{C0}^2 V_{C2}^2 (1+\gamma_{eff})^2}\left[2\eta\frac{(\gamma_0^2-1)}{\gamma_0}\gamma_{eff}^2 + \frac{(\gamma_2^2-1)^2}{4\gamma_0}\right]. \tag{34}$$

and has the same for as Eq. (31). Again note that Eq. (34) differs from the original equation in Thomsen (1999) in the isotropic term.

4.4. Accuracy and comparison

We first examine the accuracy of the four-parameter Eqs. (24), (29) and (31). We then compare the accuracy of the isotropic Eqs. (32) and (33) since they differ from each other. For the first task, we again use the model in Table 1. The moveouts calculated by the approximate equations are compared with those by ray-tracing. Fig. 3a shows the output of Eqs. (24), (29) and (31), and Fig. 3b shows the output of the isotropic equations (letting $\chi_{eff}=0$). The new approximations are accurate up to the offset-to-depth ratio (x/z) of 2.0, whilst the isotropic equations are only accurate to x/z of 1.0.

To examine the accuracy of Eqs. (32) and (33), we use the simple model of a single isotropic layer. The results are shown in Fig. 4. For comparison, we also enclose the results of the hyperbolic moveout equa-

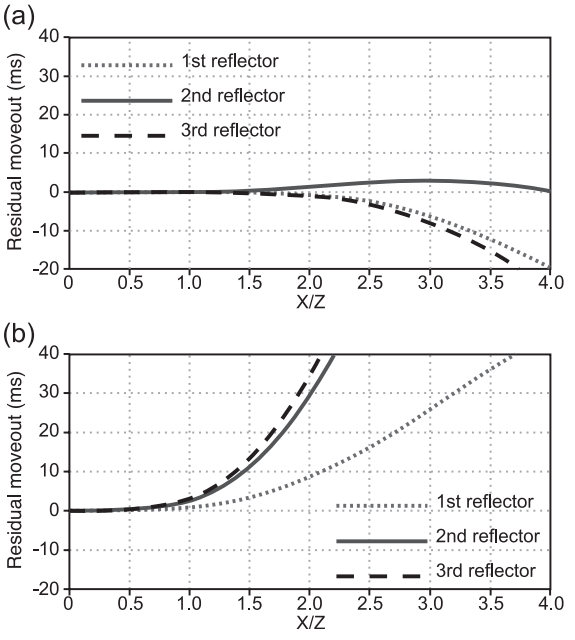

Fig. 3. Accuracy of the moveout approximations for the three-layer model in Table 1. The residual moveout is calculated as $\Delta t_C = t_C^{(exact)} - t_C^{(approx)}$, and $t_C^{(exact)}$ is calculated by ray tracing. (a) Results of the four-parameter Eqs. (24), (29) and (31), and (b) those of the isotropic equations with $\eta_{eff}=0$ and $\zeta_{eff}=0$ from Thomsen (1999). The horizontal axis is the offset-to-depth ratio, and the vertical axis is the residual moveout. The dotted line is from the first reflector, the solid line from the second reflector and the dashed line from the third reflector.

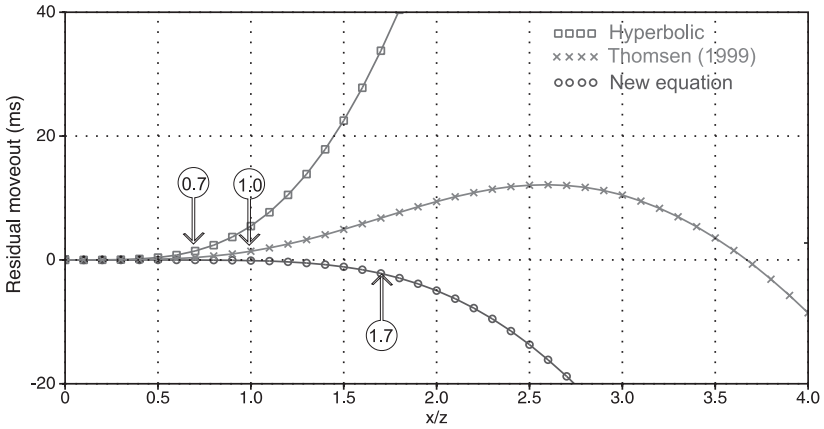

Fig. 4. Accuracy of moveout approximation for a single isotropic layer with $V_P = 2500$ m/s, $\gamma_0 = 2.5$ and depth at 1000 m. The three approximations are: squares—hyperbolic, crosses—Eq. (33) derived by Thomsen (1999) and circles—new Eq. (32). The residual moveout is calculated as $\Delta t_C = t_C^{(\text{exact})} - t_C^{(\text{approx})}$, and $t_C^{(\text{exact})}$ is calculated by ray tracing.

tion. We can see that the hyperbolic moveout equation is accurate up to $x/z = 0.7$, and the original Thomsen equation is accurate to $x/z = 1.0$, whereas the new equation is accurate up to $x/z = 0.7$. Note that, for multilayer media, the new equations are more accurate than for the single-layer case.

5. Influence of anisotropy on converted-waves

VTI influences both the position of the conversion point and converted-wave moveout. This influence comes from two sources, the P-wave anisotropy described by η or η_{eff} and the S-wave anisotropy described by ζ or ζ_{eff}. One intriguing question is whether the effects of anisotropy seen in the converted-wave are mainly from the P-wave leg, the S-wave leg or both. This has implications in parameter estimation. For examples, if the converted-wave anisotropy is mainly from the P-wave leg, then we may still not be able to recover all the necessary anisotropic information even if both P-wave and converted-wave are available. With the above analytical equations, it is possible to gain some insight into this problem.

5.1. P-wave anisotropy vs. S-wave anisotropy

For simplicity, we consider the single-layer case. We represent the anisotropic effects using the corresponding terms in Eqs. (19) and (25) for P- and S-waves, respectively. For example, for conversion-point calculation, the corresponding term representing the P-wave anisotropic effect is $\eta\gamma_0\gamma_{\text{eff}}^2$ (Eq. (19)) and, for moveout, the P-wave anisotropic term is $\eta\gamma_0\gamma_{\text{eff}}^2$. In both cases, the S-wave anisotropic term is $\zeta = \eta\gamma_{\text{eff}}^2$. Therefore, for anisotropic materials with γ_{eff} close to 1.0, the ratio of the anisotropic contributions from P- and S-waves is close to γ_0. Table 2 lists these terms for three materials, Dog Creek shale, Pierre shale and Taylor sandstone. It can be seen that the P-wave anisotropic term is about γ_0 times larger than that of the S-wave in both conversion-point and moveout calculations. The only exception is the calculation of conversion point x_C for Pierre shale, where the S-wave anisotropic term is stronger. Note that Pierre shale has a negative σ, giving rise to a γ_{eff} larger than γ_0, which is relatively rare in published measurements (Thomsen, 1986).

In multilayered media, η and ζ are replaced by η_{eff} and ζ_{eff}. From their definitions in Eqs. (16) and (17),

Table 2
Influence of *P*- and *S*-wave anisotropy on converted wave in single-layered medium

Material	x_C—Eq. (19)		t_C—Eq. (25)	
	$\eta\gamma_0\gamma_{\text{eff}}$	$\zeta = \eta\gamma_{\text{eff}}^2$	$\eta\gamma_0\gamma_{\text{eff}}^2$	$\zeta = \eta\gamma_{\text{eff}}^2$
Dog Creek shale	0.282	0.154	0.335	0.154
Pierre shale	− 0.434	− 0.932	− 2.06	− 0.932
Taylor sandstone	0.248	0.113	0.214	0.113

both η_{eff} and ζ_{eff} are combinations of the layering effect and interval anisotropy. However, as follows from the definition of η_{eff}, the layering effect and interval η_i reinforce each other, and thus η_{eff} generally increases with depth, as shown in the three-layer model in Table 1. In contrast, for ζ_{eff}, the layering effect and interval ζ_i have opposite signs, and thus cause ζ_{eff} to decrease with depth (Table 1).

In summary, the P-wave anisotropic term appears to be larger than the S-wave anisotropic term, particularly for moveout calculation. From the cases we examined, the ratio of P- to S-wave anisotropic terms is close to the vertical velocity ratio γ_0. Thus, it may be possible to recover S-wave anisotropic information from converted-wave data.

5.2. Conversion-point vs. moveout

As shown Fig. 2b, if anisotropy is ignored in the calculation of the conversion point (letting $\eta_{\text{eff}}=0$ and $\zeta_{\text{eff}}=0$), the isotropic Eq. (22) is only accurate for offsets up to half the reflector depth ($x/z=0.5$). In comparison, if anisotropy is ignored in the moveout calculation, the isotropic equation is still accurate for offsets up to the reflector depth ($x/z=1.0$), as shown in Fig. 3b. This shows that VTI has a stronger influence on the conversion point than on moveout. This can also be explained from the analytical equations. As shown in Eq. (19), P-wave anisotropy (η_{eff}) and S-wave anisotropy (ζ_{eff}) reinforce each other in determining the conversion point, whilst they have opposite signs in Eq. (25). This further increases the anisotropic influence on the calculation of the conversion point, which may lead to mis-positioning of reservoir formations.

6. Implications for parameter estimation

The above expressions for converted-wave kinematic include three kinds of parameters: medium

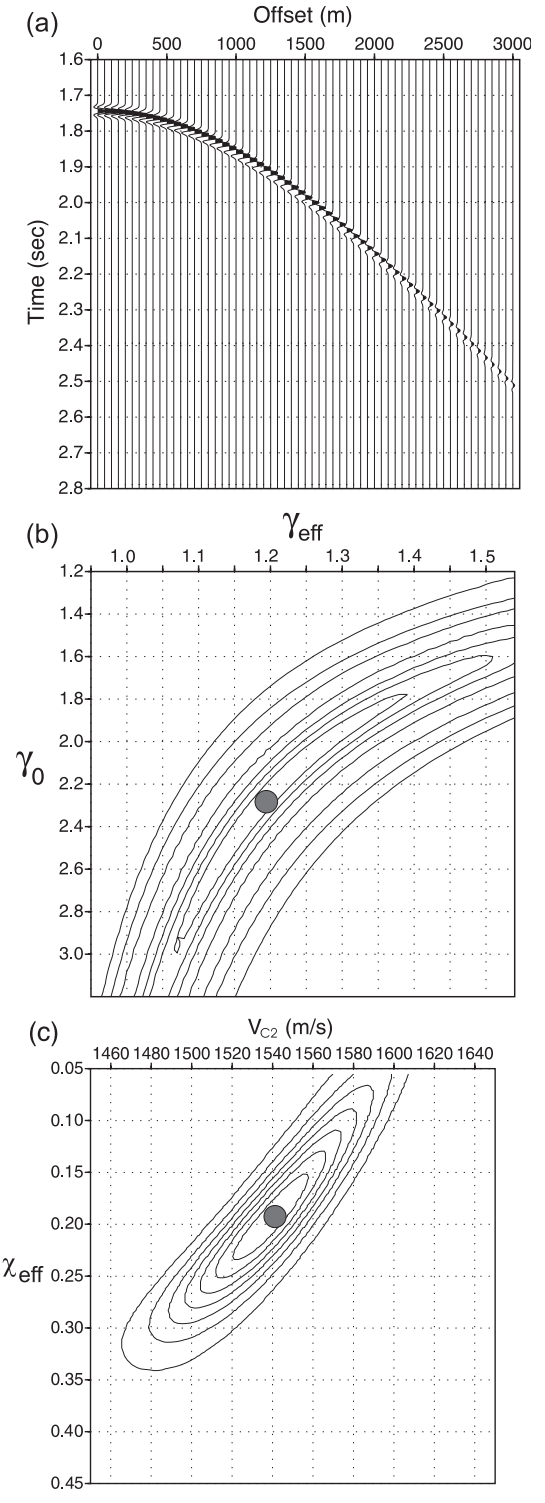

Fig. 5. Sensitivity analysis for a single VTI layer of Dog Creek shale ($V_{P0}=1875$ m/s, $V_{S0}=826$ m/s, $\epsilon=0.225$ and $\delta=0.1$) at depth $z=1000$ m. (a) Synthetic gather. (b) Double-scanning for γ_0 and γ_{eff} by fixing V_{C2} (1540 m/s) and χ_{eff} (0.187). (c) Double-scanning for V_{C2} and χ_{eff} by fixing γ_0 (2.270) and γ_{eff} (1.191). The dots indicate model results.

parameters, conversion-point attributes and moveout attributes. The medium parameters may include the P- and S-wave stacking velocities V_{P2} and V_{S2}, vertical velocity ratio γ_0, and P- and S-wave anisotropic parameters η_{eff} and ζ_{eff}. Note that the four generic Thomsen parameters are also medium parameters which are required for depth processing. The C-wave moveout attributes may include V_{C2} and χ_{eff}, whilst γ_{eff} is a conversion-point attribute. With this kind of parameterization, the issue is how to estimate the stacking velocity model V_{C2}, γ_0, γ_{eff} and χ_{eff} using the new equations. Here, we examine the sensitivity to the parameters, and investigate the viability of the double-scanning procedure for parameter estimation.

6.1. Sensitivity analysis of velocity ratios γ_0 and γ_{eff}

In general, the C-wave moveout is not sensitive to variations of γ_0 and γ_{eff} (Li and Yuan, 2001). Fig. 5a and b illustrate whether or not the two velocity ratios can be resolved by semblance analysis with sufficient resolution and accuracy, where we assume known V_{C2} and χ_{eff} and directly invert for γ_0 and γ_{eff}. Synthetic modelling (Fig. 5a) is generated by ray tracing for the Dog Creek shale, and the depth of reflector is 1000 m, maximum offset is 3000 m, and a 30 Hz Ricker's wavelet is used. Eq. (24) is used for inversion, where the exact V_{C2} and χ_{eff} values are used as inputs. The traces are stacked for semblance analysis as shown in Fig. 5b. The resolutions of semblance analysis for both γ_0 and γ_{eff} are poor. Tests have also been carried out for other materials (Pierre shale and Taylor sandstone; Yuan, 2002) and all materials studied show poor resolution when determining γ_0 and γ_{eff} from semblance analysis. These results indicate that γ_0 and γ_{eff} may be difficult, if not impossible, to obtain from C-wave moveout inversion. On the other hand, if γ_0 and γ_{eff} are fixed, double scanning for V_{C2} and χ_{eff} shows good resolution and correct results (Fig. 5c).

6.2. Estimating γ_0 and γ_{eff}

The previous results suggest that γ_0 and γ_{eff} can not be determined from C-wave reaction moveout, and that correlation of P- and C-wave sections is likely the only means to obtain a reliable γ_0 in the absence of other independent information. The next question is how to estimate γ_{eff}?

First, from the conversion-point Eqs. (13), (18) and (19), one can see that γ_{eff} is separated from other parameters in the first order term. Thus, γ_{eff} can be reliably determined from the conversion-point signature provided the signature can be estimated from the data. This forms the basis of the CCP scanning technique (Bagaini et al., 1999). Unfortunately, the conversion-point signature can only be estimated in the presence of certain geological features, such as the apex of an anticline, a fault or a dipping layer.

Secondly, if V_{P2}, V_{C2} and γ_0 are known, γ_{eff} may be determined from Eq. (6). However, error propagation

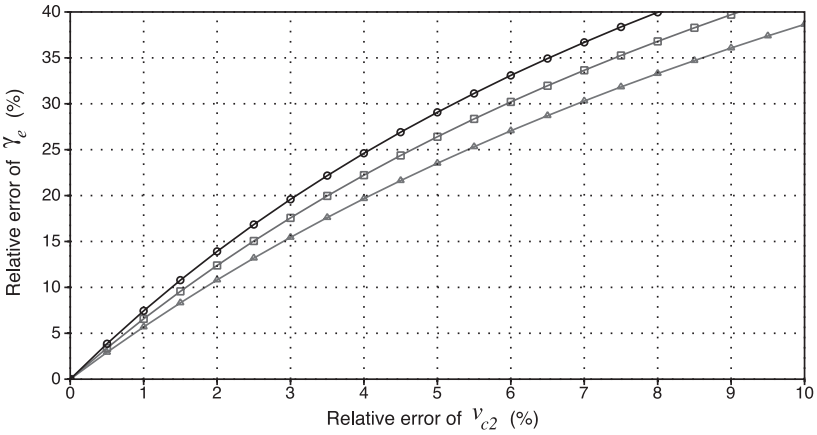

Fig. 6. Error propagation from estimated V_{C2} to γ_{eff}. Three curves indicate different velocity ratios V_P/V_S: 2.0 (triangles), 2.5 (squares) and 3.0 (circles), respectively.

is known to be a problem for this approach. Normally, V_{P2} can be determined rather precisely from *P*-wave data when signal-to-noise ratio is reasonable, whereas errors are often associated with V_{C2}, and will propagate into γ_{eff} through Eq. (6).

Fig. 6 shows the error propagation from V_{C2} to γ_{eff} for different velocity ratios. A 3% error in V_{C2} will result in 15–20% errors in γ_{eff} when the average velocity ratio varies from 2.0 to 3.0. Thus, the use of Eq. (6) for estimating γ_{eff} requires accurate determination of V_{C2} with errors less than 2%, assuming a 10% error margin in γ_{eff}.

6.3. Double-scanning in layered VTI media

Here we use the three-layer model in Table 1 to demonstrate the viability of the double-scanning procedure in layered media. We assume that γ_0 was obtained by correlating P- and C-wave stacked sections, and γ_{eff} was found from Eq. (6), where the P-wave moveout velocity V_{P2} can be determined from P-wave data. Fig. 7a is a synthetic gather calculated by ray tracing for the three-layer model in Table 1. Fig. 7b–d shows the results of semblance analyses for V_{C2} and χ_{eff}, using γ_{eff} and γ_0 as a priori information.

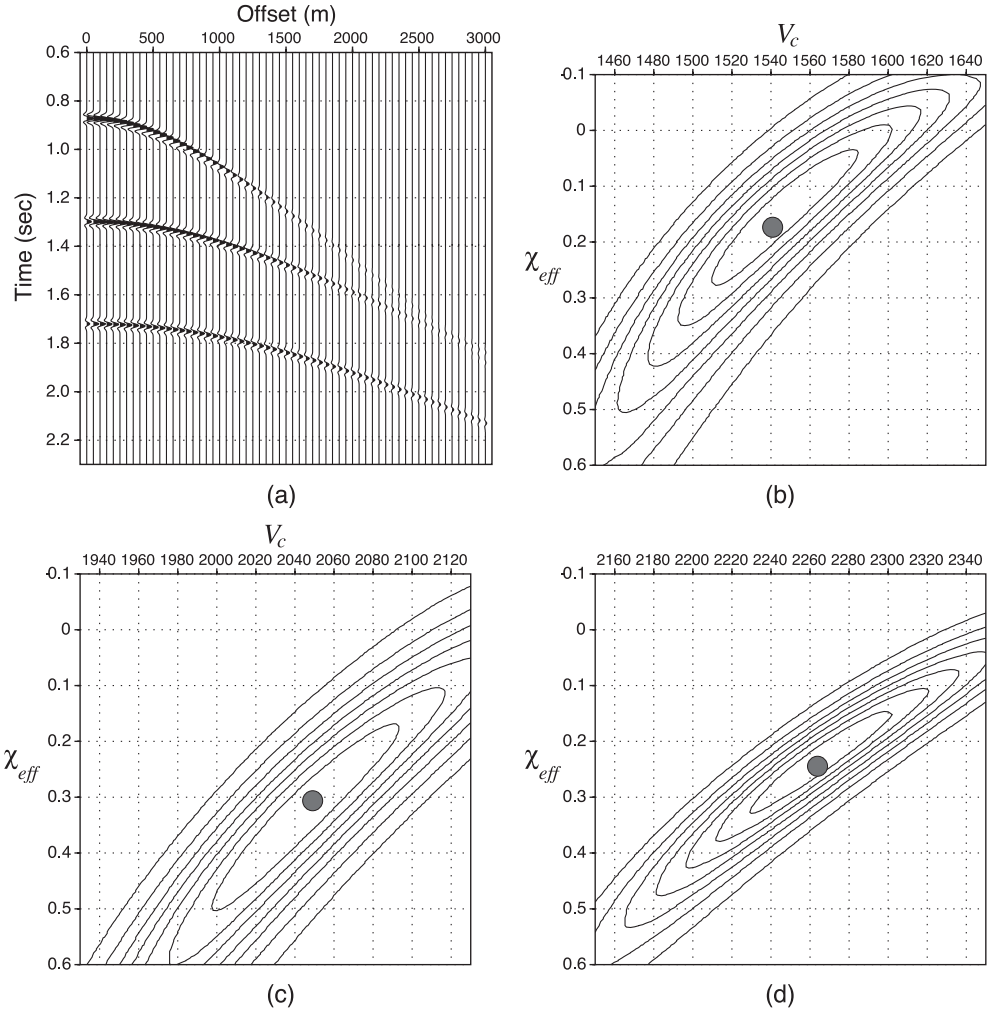

Fig. 7. Semblance analysis for V_{C2} and χ_{eff} with a priori information about γ_0 and γ_{eff} for a given t_{C0}, using the three-term moveout Eq. (24). The circles are model values of V_{C2} and χ_{eff}. (a) Synthetic seismogram from ray tracing and semblance analysis for the (b) first reflector, (c) second reflector and (d) third reflector.

The offset range used for semblance analysis is limited to an offset-to-depth ratio of 2.0. The circles are the exact values of V_{C2} and χ_{eff}. The semblance spectra show high resolution and good inversion results for V_{C2} and χ_{eff}.

Note that it may be easy to confuse the issues of moveout correction and parameter estimation. Moveout correction itself can be accomplished using the generic form of Tsvankin and Thomsen (1994) with the coefficients determined by semblance analysis. In contrast, parameter estimation requires accurate analytical expressions for the relevant moveout coefficients, and this is the main purpose of this paper.

6.4. Error analysis

The above analysis shows that the modified moveout Eqs. (24), (29) and (31) allow the use of existing P-wave semblance procedures, as developed by Grechka and Tsvankin (1988), for C-wave moveout analysis and parameter estimation. Grechka and Tsvankin (1988) also gave a detailed account of the effects of correlated travel-time errors on non-hyperbolic moveout analysis. They showed that random travel-time errors have very little influence on the results of semblance analysis. In contrast, correlated travel-time errors can have a significant effect, although they may not affect the resolution of the semblance analysis. These findings are expected to hold for C-wave moveout analysis as well.

7. Single-scanning for estimating V_{C2} and χ_{eff}

The double-scanning procedure may be robust, but may also be time-consuming. Thus, it is worth to investigate the use of single-scanning procedure for parameter estimation. For this, the accuracy of V_{C2} is essential. V_{C2} is the short-spread NMO stacking velocity, but it often cannot be determined accurately using conventional hyperbolic procedures.

7.1. Single-scanning for V_{C2}

Here, we introduce a simple single-scanning procedure over the intermediate offsets (offset-depth ratio up to $x/z=1.5$) for determining V_{C2} accurately. The procedure utilizes a background γ to quantify the non-hyperbolic moveout over the intermediate offsets. The C-wave moveout over intermediate offsets up to $x/z=1.5$ may be expressed as, with a background velocity ratio γ (Yuan, 2002),

$$t_C^2 = t_{C0}^2 + \frac{x^2}{V_{C2}^2} - \frac{(\gamma-1)^2}{\gamma V_{C2}^2}\frac{x^4}{4t_{C0}^2 V_{C2}^2 + (\gamma-1)x^2}. \tag{35}$$

Thus, if a background velocity ratio γ is given, we may use Eq. (35) for velocity analysis. We test this idea using the synthetic data in Fig. 7a, and the single-scanning results of V_{C2} are shown in Fig. 8. The errors in hyperbolic analysis are about 3% over offsets up to $x/z=1.0$ (Fig. 8a), whilst those in the non-hyperbolic analysis are less than 1% over offsets up to $x/z=1.5$ (Fig. 8b and c).

To check the influence of the background velocity ratio on velocity analysis, a velocity ratio of 2.0 is used in Fig. 8b, whilst a velocity ratio of 3.0 is used in Fig. 8c. Comparing Fig. 8b with Fig. 8c shows that 20% change in velocity ratio does not affect V_{C2} scanning results very much. The insensitivity of C-wave moveout signature to the velocity ratios over intermediate offsets means that for velocity analysis purposes, detailed knowledge about the velocity ratio is not necessary. The differences between γ_0 and γ_{eff} can also be ignored. This justifies the use of a homogeneous and isotropic Eq. (35) for non-hyperbolic moveout analysis over intermediate offsets.

7.2. Single-scanning for χ_{eff}

The previous section shows that it is possible to determine V_{C2} accurately from intermediate offsets using non-hyperbolic velocity analysis. Thus, with V_{C2}, γ_0 and γ_{eff} all determined, it may be possible to determine χ_{eff} by a single-scanning technique from the far offset C-wave data affected by χ_{eff}. Here, we use the three-layer model in Figs. 7a and 8 to test this idea. Fig. 9 shows the results with good resolution and accuracy. However, this single-scanning technique is very sensitive to the accuracy of V_{C2}. A 2% perturbation in V_{C2} gives about 15% changes in χ_{eff}. Note here the input V_{C2} is 2% higher than the exact values, which gives the χ_{eff} curve a constant shift toward the

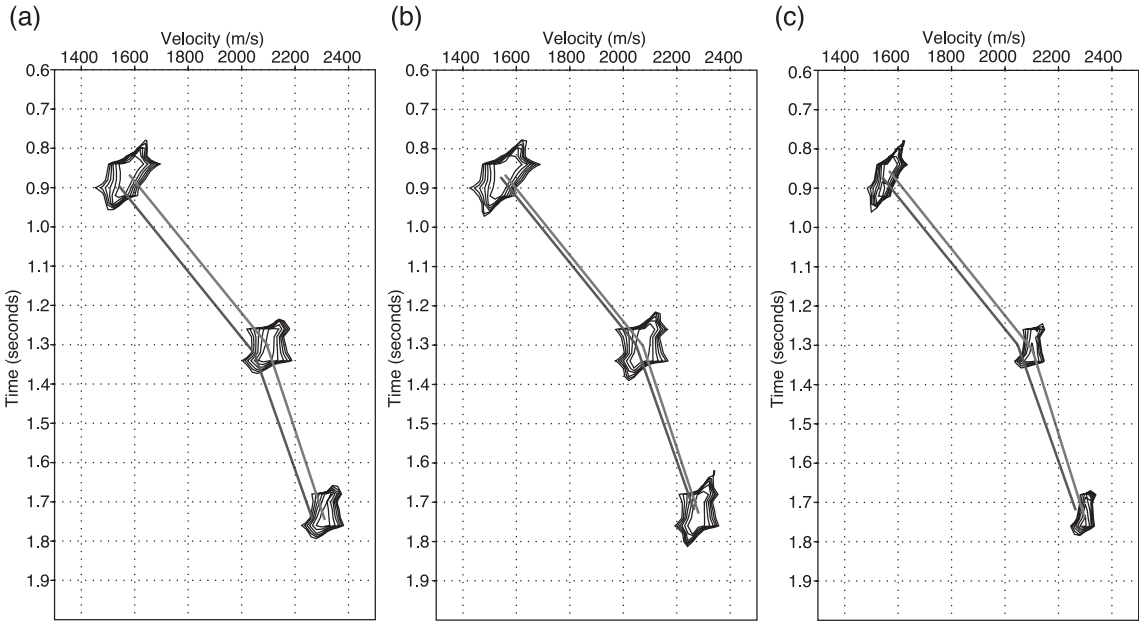

Fig. 8. Accuracy of hyperbolic and non-hyperbolic velocity analysis for the three-layer VTI model in Table 1. (a) Hyperbolic velocity analysis with $x/z = 1.0$. (b) Non-hyperbolic analysis with $x/z = 1.0$ and $\gamma = 2.0$, and (c) the same as (c) but for $x/z = 1.5$ and $\gamma = 3.0$.

isotropic direction. This is similar to the results of Grechka and Tsvankin (1988) for P-wave moveout data analysis. Considering that χ_{eff} is a small quantity, the errors are quite reasonable. For example, assuming $\chi_{eff} = 0.3$, a 15% changes indicate an error of 0.045, which implies a 4% or 5% over- or underestimate of

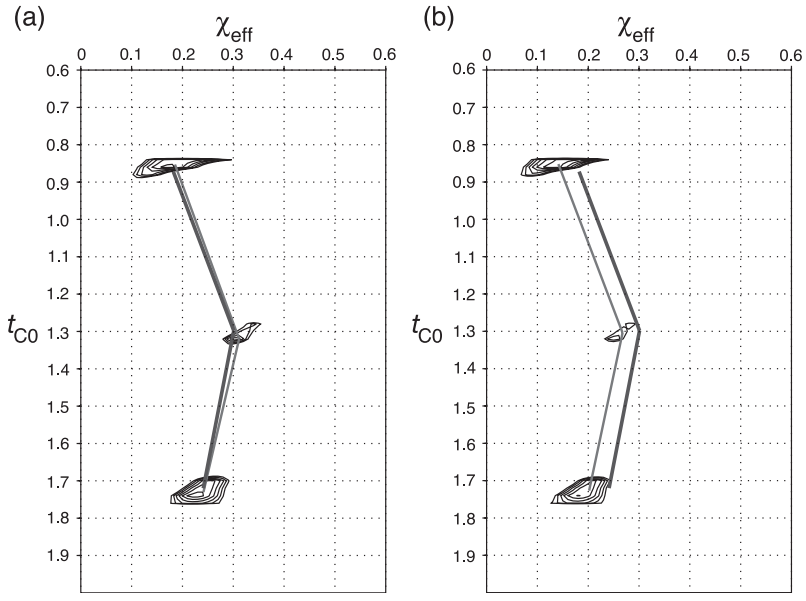

Fig. 9. Accuracy of semblance analysis for χ_{eff} for the data in Fig. 8a: (a) with exact inputs of V_{C2}, γ_0 and γ_{eff}. (b) The same as (a) but given 2% perturbation in V_{C2}, and exact inputs of γ_0 and γ_{eff}. The thick line is for model values, and the thin line for picked values.

the anisotropy. Still, due to trade-offs between V_{C2} and χ_{eff}, the single-scanning procedures have to be used carefully.

8. Work flows for anisotropic velocity analysis

From the above theoretical and numerical analyses, two possible work flows can be suggested to determine the stacking velocity model (V_{C2}, γ_0, γ_{eff} and χ_{eff}) using 4C seismic data: a double-scanning work flow and a single-scanning work flow.

8.1. The double-scanning work flow

In the numerical analysis, we used γ_0 and γ_{eff} as input parameters for the double-scanning algorithm. In real data processing, it may be more convenient to use V_{P2} to replace γ_{eff} as the input parameter. During the scanning process, for each given set of V_{P2}, V_{C2} and γ_0, the corresponding γ_{eff} can be calculated using Eq. (6). This increases the computation of double scanning, but simplifies the work flow and reduces the number of iterations. (The flow involves one iteration for V_{C2} due to the requirement for correlation to obtain γ_0.) With this in mind, the work flow can be designed as follows.

The first step is to process the P-wave data and build the P-wave velocity model V_{P2}. This is independent of the C-wave data. Standard methods may be used to obtain the best imaging and the velocity model.

The second step is to obtain γ_0 through an initial processing of the C-wave data and a coarse correlation with the P-wave data. The main purpose of the C-wave processing is to obtain a brute stack for correlation with the P-wave section. The key information to preserve during processing is the time t_{C0}. Thus, standard hyperbolic processing can be used and the C-wave data may even be processed in the CDP domain. Care should be taken to limit the data to the short offsets up to $x/z=1.0$. The third step is to determine V_{C2} and χ_{eff} by the double-scanning procedure on selected horizons using V_{P2} and γ_0 as input parameters. The final step is to determine γ_{eff} using Eq. (6) from V_{P2} and V_{C2}. Note that here V_{C2} is the double scanning result. During the initial processing of the C-wave data, an initial estimate of V_{C2}^* is also obtained from hyperbolic analysis; this V_{C2}^* should be ignored.

8.2. The single-scanning work flow

This flow also has four steps. The first step is the P-wave processing and is the same as that in the double scanning work flow.

The second step is to obtain accurate estimates of V_{C2} by non-hyperbolic velocity analysis using Eq. (35). The C-wave data is processed in the ACCP Asymptotic Common Conversion Point domain with a background γ. After ACCP binning, non-hyperbolic velocity analysis with the same γ is employed to determine V_{C2} and to generate a C-wave stacked section. The data have to be limited to the intermediate offsets up to $x/z=1.5$. The third step is to estimate γ_0 and γ_{eff}. As before, γ_0 is estimated by a coarse correlation of the P- and C-wave stacked sections, and γ_{eff} is obtained from Eq. (6) using V_{P2}, V_{C2} and γ_0 as inputs.

Once V_{C2}, γ_0 and γ_{eff} are determined, the final step is to obtain χ_{eff} by single-scanning semblance analysis as shown in Fig. 9 over the entire offsets up to $x/z=3.0$.

This work flow is more efficient in real data processing. However, the single-scanning results of χ_{eff} has an error margin of 15–20% depending on the accuracy of V_{C2}, as shown in the synthetic test (Fig. 9), and this trade-off may invalidate the single-scanning procedure.

9. Field data example

The above work flows have been applied to several 4C datasets from the North Sea including Guillemot, Alba and Valhall; here, we use the Guillemot 4C data (courtesy of Shell Expro). Details of acquisition geometry of this dataset were documented in Yuan et al. (1998) and standard P- and C-wave wave processing can also be found in Yuan et al. (1998) and Li and Yuan (1999).

We select the gathers at CCP (or CDP) 1100 to illustrate anisotropic velocity analysis. In this context, CCP and CDP are co-located. Fig. 10 shows the P- and C-wave data at location CCP 1100. A background γ of 2.5 was used to obtain the CCP

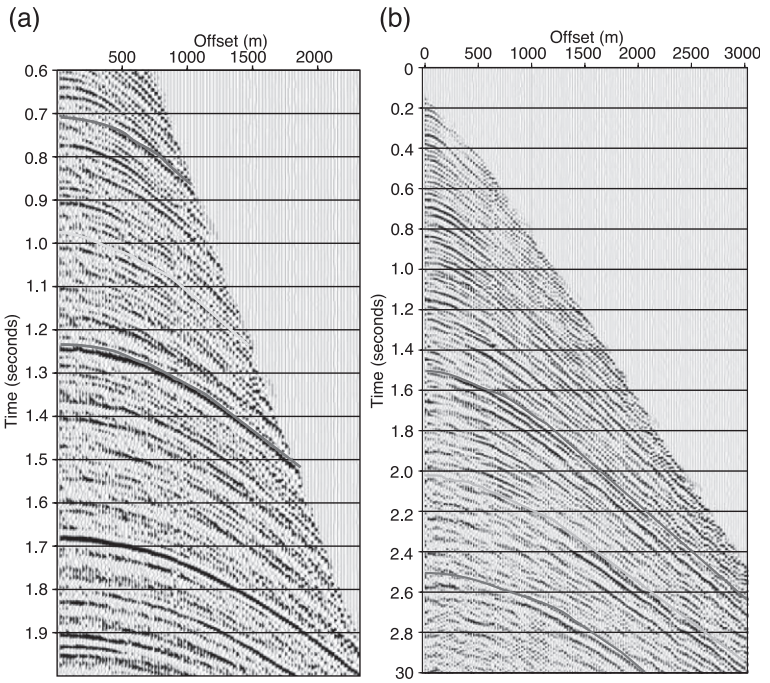

Fig. 10. (a) P-wave CDP gather at CDP 1100 of the Guillemot data and (b) the corresponding C-wave gather at CCP 1100. CDPs and CCPs are co-located. The solid lines mark some horizons correlated by Yuan et al. (1998).

gather. Some correlated horizons based on previous work (e.g., Yuan et al., 1998; Li and Yuan, 1999) are marked on the data. The overall quality of this dataset is excellent, and the processing of both P- and C-wave is straightforward. The estimated P-wave stacking velocity V_{P2} and vertical velocity ratio γ_0 at CDP or CCP location 1100 (both obtained by conventional processing) are listed in Table 3 for the three correlated events in Fig. 10. Next, using these as a priori information, we examine the sensitivity of double-scanning, the accuracy of non-hyperbolic velocity analysis, and the effectiveness of single-scanning.

9.1. Double scanning for V_{C2} and χ_{eff}

The three correlated events at $t_{C0}=1520$, 2050 and 2570 ms (Fig. 10) are selected to illustrate the double-scanning processing. The input parameters are V_{P2} and γ_0 and are listed in Table 3. Good resolution in V_{C2} and χ_{eff} is obtained, and values picked from Fig. 11a–c are listed in Table 3. The average χ_{eff} is about 0.22, indicating a significant amount of converted-wave anisotropy.

To test the sensitivity of double-scanning to errors in the input parameters, we add 10% errors to the input γ_0, and the corresponding double scanning

Table 3
V_{C2}, γ_{eff} and χ_{eff} obtained from the double-scanning work flow (Fig. 11) and single-scanning work flow including non-hyperbolic velocity analysis for V_{C2} (Fig. 12) and single scanning for χ_{eff} (Fig. 14)

No.	t_{C0} (ms)	t_{P0} (ms)	V_{P2} (ms)	γ_0	Double scanning			Single scanning (non-hyperbolic)		
					V_{C2} (m/s)	γ_{eff}	χ_{eff}	V_{C2} (m/s)	γ_{eff}	χ_{eff}
1	1531	707	1920	3.33	1130	2.00	0.16	1120	2.10	0.23
2	2064	980	2000	3.21	1165	2.33	0.26	1190	2.04	0.21
3	2574	1243	2047	3.14	1235	1.97	0.27	1240	1.93	0.28

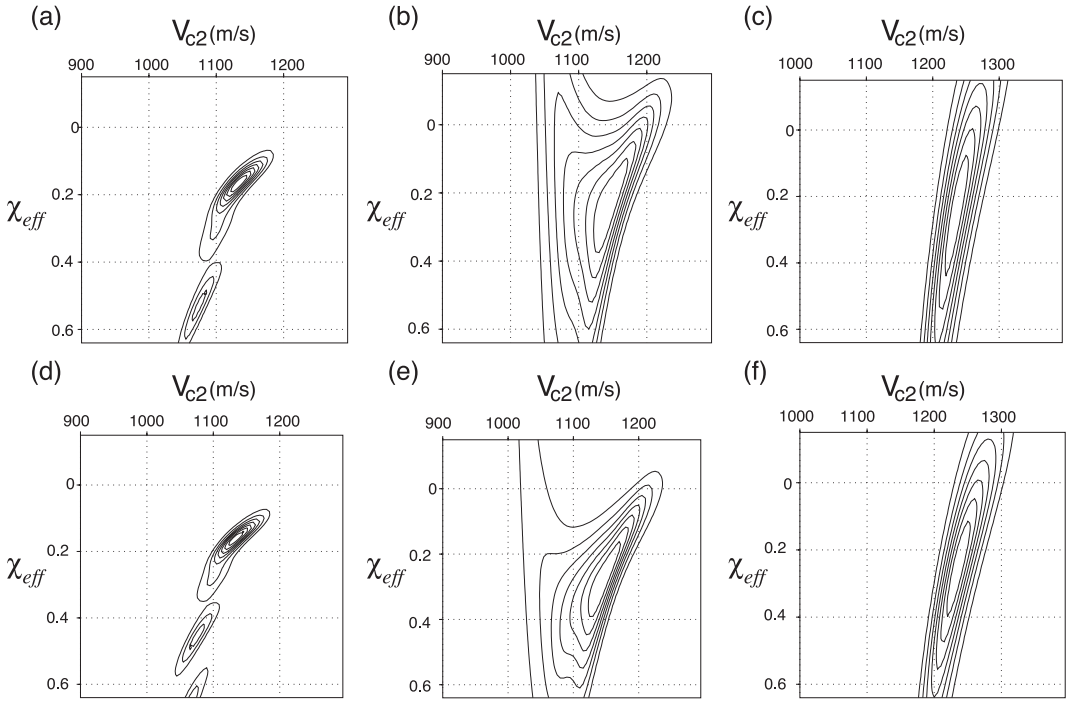

Fig. 11. Double-scanning analysis for V_{C2} and γ_{eff} using a priori information for V_{P2} and γ_0 for the data in Fig. 10b. V_{P2} and γ_0 are listed in Table 3. Events at (a) $t_{C0}=1520$ ms, (b) $t_{C0}=2050$ ms and (c) $t_{C0}=2570$ ms. (d), (e) and (f) are the same as (a), (b) and (c), but there are 10% errors added to the corresponding γ_0.

results are shown in Fig. 11d–f. The errors in γ_0 have almost no effect on V_{C2}, but there are about 15% differences in the values of χ_{eff}.

9.2. Non-hyperbolic velocity analysis for V_{C2}

Eq. (35) has been used to perform non-hyperbolic velocity analysis with the same background $\gamma=2.5$ as ACCP binning. The offsets are limited to the intermediate range up to $x/z=1.5$ in order to determine V_{C2}. Fig. 12a shows the semblance spectra for the CCP gather in Fig. 10b. Fig. 12b shows the corresponding hyperbolic spectra for comparison. The two lines show a possible picking error of 2%. The quality of the spectra obtained by non-hyperbolic velocity analysis is substantially improved in terms of the signal-to-noise ratio. There are 5–7% differences between the non-hyperbolic and hyperbolic results (Fig. 12). The difference in velocities is substantial and is due to the significant non-hyperbolic moveout enhanced by the presence of anisotropy.

9.3. Verifications and comparisons

There are 1–2% differences between the V_{C2} from double scanning and those from non-hyperbolic velocity analysis (Table 3). They both differ from the hyperbolic V^*_{C2} significantly. To examine the accuracy of these velocities, we use them to perform moveout correction by Eq. (24), and the results are shown in Fig. 13. Most events are substantially under-corrected when the hyperbolic velocities V^*_{C2} are used for moveout correction, confirming that V^*_{C2} is too high (Fig. 13b). In contrast, most of the events are properly aligned when using the non-hyperbolic velocity (Fig. 13a), except for the events at $t_{C0}=1.6$ s and $t_{C0}=2.1$ s, which are slightly over-corrected. In Fig. 13a and b, χ_{eff} is set to zero. Note that those events at $t_{C0}=1.6$ s and $t_{C0}=1.6$ s can also be aligned with corresponding χ_{eff} values of 0.16 and 0.26 (Fig. 13c). This shows that the χ_{eff} has accurately captured the anisotropic effects in the data.

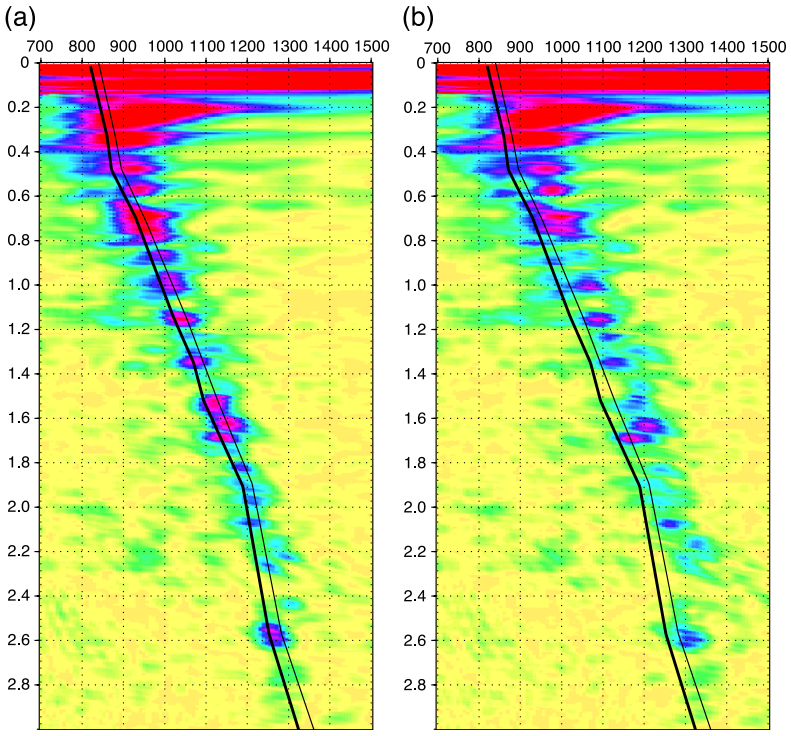

Fig. 12. Comparison of (a) non-hyperbolic with (b) hyperbolic velocity analyses for the intermediate offsets up to $x/z = 1.5$. The lines show a possible picking error of 2%.

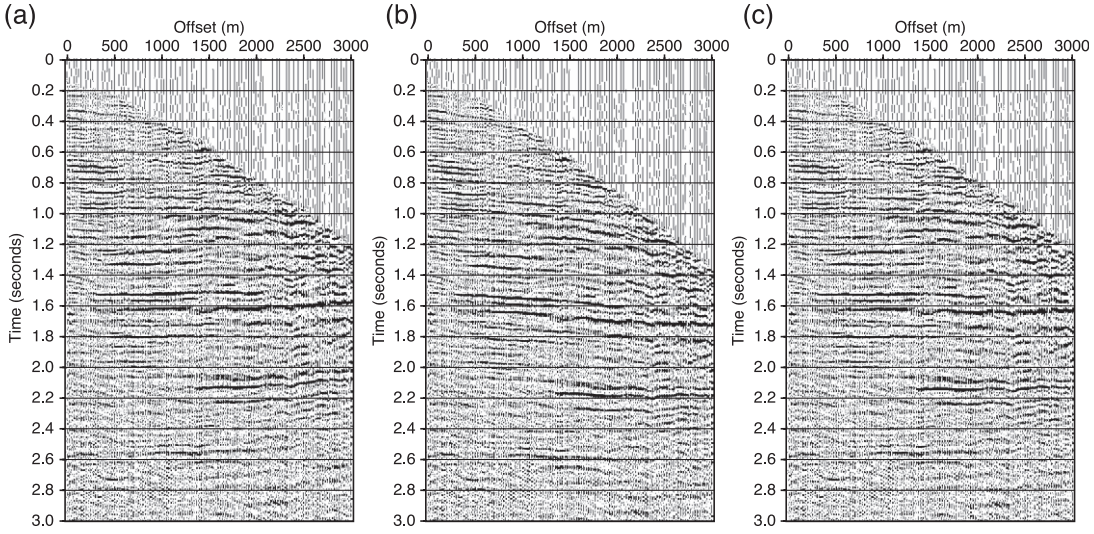

Fig. 13. Comparison of C-wave moveout correction using different values of V_{C2}. γ_{eff} and χ_{eff} with γ_0 fixed as in Table 3: (a) $\chi_{eff} = 0$ and V_{C2} and γ_{eff} from the non-hyperbolic velocity analysis in Fig. 12a; (b) the same as in a but V_{C2} and γ_{eff} from the hyperbolic velocity analysis in Fig. 12b; (c) the same as in (a) but χ_{eff} from the double-scanning analysis in Fig. 11.

9.4. γ_{eff} and single-scanning results

There are two sets of V_{C2}, which can be used to determine the γ_{eff}: the double-scanning V_{C2} and the non-hyperbolic V_{C2}. The corresponding values γ_{eff} are shown in Table 3. For the second event at $t_{C0}=2064$ ms, there are 15% differences in γ_{eff}; for the first and third events, the difference is small.

Fig. 14 shows the results of single-scanning for χ_{eff} with both sets of V_{C2} and γ_{eff} for comparison. For most of the shallow section above 1.5 s, there is no resolution of χ_{eff}. This agrees with the results in Fig. 13 where the events in the shallow part are aligned well with an assumption of $\chi_{eff}=0$. For the section between 1.5 and 2.6 s, the spectra show good resolution for χ_{eff}. The picked χ_{eff} agree well with the results of double scanning. Also note that χ_{eff} spectra show a moderate 20% of difference in χ_{eff} between the input of non-hyperbolic V_{C2} and the input of double scanning V_{C2}. Large differences up to 40% are observed for the event at 2.1 s. Overall, the single-scanning χ_{eff} analysis can be used for real data processing. Since the two sets of results are not very different, and the non-hyperbolic V_{C2} and the single-scanning of χ_{eff} are better defined vertically, we recommend the single-scanning work flow. However, applications to other datasets do sometimes show limited resolution in χ_{eff}, and double-scanning may still be needed as a quality control procedure.

10. Discussion and conclusions

We have derived analytical expressions for calculating the P-SV conversion point in layered VTI media. These expressions are extensions of those in Thomsen (1999), but are derived using the Taylor-series expansion of the conversion-point equation, and are accurate for large offsets up to three times the reflector depth ($x/z=3.0$). [The existing equations used in the industry are only valid to about half the reflector depth ($x/z=0.5$).] This ensures accurate binning of long-offset data in the presence of anisotropy. The new equations, with increased accuracy, may help

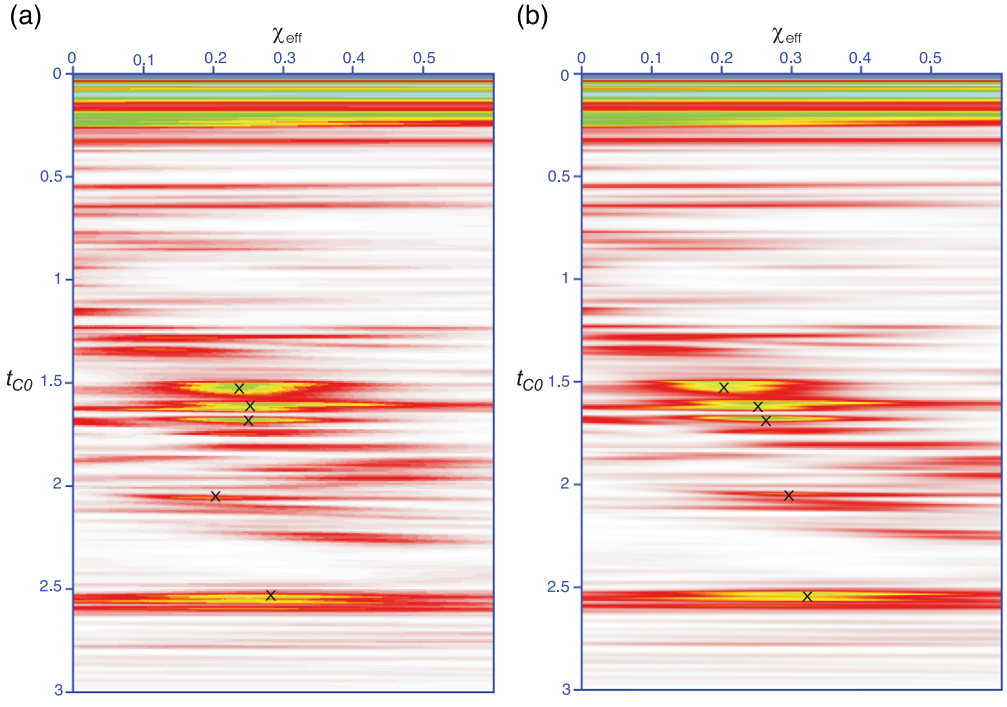

Fig. 14. Semblance analysis for χ_{eff} applied to the data in Fig. 10b: (a) with non-hyperbolic V_{C2} and the corresponding γ_{eff}, and (b) with double scanning V_{C2} and the corresponding γ_{eff} for comparison.

to estimate anisotropy at locations with distinct geological features, such as fault points (Yuan and Li, 2002).

We have presented modified equations of Tsvankin and Thomsen (1994) for calculating converted-wave travel-times in layered VTI media in order to utilize the existing semblance analysis procedures for parameter estimation. These equations are accurate up to offsets twice the reflector depth ($x/z=2.0$), as compared to just $x/z=1.0$ of those modified equations in Thomsen (1999). The new equation uses four parameters to describe the C-wave moveout: the converted-wave stacking velocity V_{C2}, vertical velocity ratio γ_0, effective velocity ratio γ_{eff} and a new anisotropic parameter χ_{eff}.

We have also discussed the application of these equations for determining the C-wave stacking velocity model described by V_{C2}, γ_0, γ_{eff} and χ_{eff}, and demonstrated the application using both synthetic and real data. With a priori knowledge of the vertical and effective velocity ratios γ_0 and γ_{eff}, the C-wave stacking velocity V_{C2} and the anisotropic parameter χ_{eff} may be estimated from far-offset C-wave data using either a double-scanning or a single-scanning procedure. Real data applications show that the double-scanning is robust but time-consuming. The single-scanning flow with non-hyperbolic velocity analysis for V_{C2} may provide an alternative. The non-hyperbolic velocity analysis has a similar accuracy to that of the double-scanning analysis, and χ_{eff} obtained from single-scanning semblance analysis agrees with the double scanning results in most cases. However, care should be taken with the single-scanning procedure due to the trade-offs between parameters.

We conclude that the newly derived expressions have captured the conversion-point and moveout signatures in terms of measurable moveout attributes for mid-to-long offset data. An anisotropic parameter χ_{eff} is introduced to quantify the anisotropic effects on the C-wave reflaction moveout, and another coefficient ζ_{eff} is introduced to quantify the anisotropic effects in the S-wave leg of a C-wave ray. In a single-layered VTI medium, $\chi_{eff}=\chi=\gamma_0\gamma_{eff}^2\eta-\zeta=(\gamma_0-1)\gamma_{eff}^2\eta$, and $\zeta_{eff}=\zeta=\gamma_{eff}^2\eta$. The derived equations enable the use of conventional procedures such as semblance analysis and Dix-type model building to implement anisotropic processing, and make anisotropic processing affordable.

Acknowledgements

We thank Leon Thomsen for useful discussion. We thank Shell Expro for providing the Guillemot data and for permission to show the data. The data was original provided to the University of Edinburgh industry-sponsored project *Processing of four-component Sea Floor Seismic Data* (BP, DTI, Elf, Mobil, PGS, Shell and Western Geophysical). We thank Floris Strijbos and Professor Anton Ziolkowski for agreeing to share the data with the Edinburgh Anisotropy Project (EAP). This work is funded by the EAP of the British Geological Survey (BGS) and is published with the approval of the Executive Director of the BGS and the EAP sponsors: Agip, BG, BP, ChevronTexaco, CNPC, ConocoPhillips, DTI/RIPED-LangFang, KerrMcGee, Landmark, Marathon, Norsk Hydro, PGS, Schlumberger, Texaco, TotalFinaElf, Veritas DGC.

Appendix A. Derivation of conversion-point equation in layered anisotropic media

Consider a horizontally layered medium, as shown in Fig. 1, with each layer being homogeneous and transversely isotropic with a vertical symmetry axis (VTI). v_{Pi}, w_{Pi} are the interval P-wave phase and group velocities, v_{Si} and w_{Si} are their S-wave counterparts, and Δz_i is the thickness of the i-th layer. θ_{Pi} and θ_{Si} are the angles between the group velocity vectors and the vertical axis. x_P is the conversion point offset from the source for the P-wave path, and x_S is the corresponding offset to the receiver for the shear wave path. Note that in this context, we have $x_C=x_P$.

The total offset of ray path x is

$$x = x_P + x_S, \tag{A-1}$$

where

$$x_P = \sum_{i=1}^{n} \Delta x_{Pi} = p\sum_{i=1}^{n} U_{Pi}\Delta t_{Pi};$$
$$x_S = \sum_{i=1}^{n} \Delta x_{Si} = p\sum_{i=1}^{n} U_{Si}\Delta t_{Si}; \quad U_i = \frac{w_{1i}}{p}. \tag{A-2}$$

Here, p is the horizontal component of slowness vector (the ray parameter, dt/dx for the ray emerg-

ing at offset x, Δt_i is the oblique one-way traveltime in the i-th layer, w_1 is the horizontal component of the group velocity vector. The subscripts "P" and "S" indicate terms related with P- or S-wave paths.

Because x_P is the odd function of x, Taylor series expansion of the conversion point offset x_P at total offset x can be written as

$$x_P = \lim_{x\to 0}\sum_{k=0}^{\infty} c_{2k}x^{2k+1} = \lim_{p\to 0}\sum_{k=0}^{\infty} c_{2k}x^{2k+1}, \qquad (A-3)$$

where

$$c_{2k} = \frac{1}{(2k+1)!}\frac{\mathrm{d}^{2k+1}x_p}{\mathrm{d}x^{2k+1}}.$$

A.1. Deriving Eq. (14) for c_0

When $k=0$,

$$c_0 = \lim_{p\to 0}\frac{\mathrm{d}x_p}{\mathrm{d}x} = \lim_{p\to 0}\frac{\mathrm{d}x_p}{\mathrm{d}p}\frac{\mathrm{d}p}{\mathrm{d}x}. \qquad (A-4)$$

From Eqs. (A-1) and (A-2),

$$\frac{\mathrm{d}x_p}{\mathrm{d}p}\frac{\mathrm{d}p}{\mathrm{d}x} = \frac{\sum_{i=1}^{n} U_{Pi}\Delta t_{Pi} + p\frac{\mathrm{d}}{\mathrm{d}p}\left(\sum_{i=1}^{n} U_{Pi}U_{Pi}\Delta t_{Pi}\right)}{\sum_{i=1}^{n} U_{Pi}\Delta t_{Pi} + p\frac{\mathrm{d}}{\mathrm{d}p}\left(\sum_{i=1}^{n} U_{Pi}\Delta t_{Pi}\right) + \sum_{i=1}^{n} U_{Si}\Delta t_{Si} + p\frac{\mathrm{d}}{\mathrm{d}p}\left(\sum_{i=1}^{n} U_{Si}\Delta t_{Si}\right)}, \qquad (A-5)$$

where

$$p\frac{\mathrm{d}}{\mathrm{d}p}\left(\sum_{i=1}^{n} U_{Pi}\Delta t_{Pi}\right) = p\sum_{i=1}^{n}\frac{\mathrm{d}U_{Pi}}{\mathrm{d}p}\Delta t_{Pi} + p^2\sum_{i=1}^{n} U_{Pi}^2\Delta t_{Pi}; \qquad (A-6)$$

$$p\frac{\mathrm{d}}{\mathrm{d}p}\left(\sum_{i=1}^{n} U_{Si}\Delta t_{Si}\right) = p\sum_{i=1}^{n}\frac{\mathrm{d}U_{Si}}{\mathrm{d}p}\Delta t_{Si} + p^2\sum_{i=1}^{n} U_{Si}^2\Delta t_{Si}. \qquad (A-7)$$

For a VTI medium, Tsvankin and Thomsen (1994) obtained

$$\lim_{p\to 0} U_{Pi} = v_{P2i}^2 = v_{P0i}^2(1+2\delta_i), \qquad (A-8)$$

$$\lim_{p\to 0} U_{Si} = v_{S2i}^2 = v_{S2i}^2(1+2\sigma_i), \qquad (A-9)$$

$$\lim_{p\to 0}\frac{1}{p}\frac{\mathrm{d}U_{Pi}}{\mathrm{d}p} = \lim_{p\to 0}\frac{\mathrm{d}^2U_{Pi}}{\mathrm{d}p^2} = 8v_{P0i}^4(\varepsilon_i-\delta_i)\left(1+\frac{2\delta_i}{1-\frac{v_{S0i}^2}{v_{P0i}^2}}\right), \qquad (A-10)$$

and

$$\lim_{p\to 0}\frac{1}{p}\frac{\mathrm{d}U_{Si}}{\mathrm{d}p} = \lim_{p\to 0}\frac{\mathrm{d}^2U_{Si}}{\mathrm{d}p^2} = -8v_{S0i}^4\sigma_i\left(1+\frac{2\delta_i}{1-\frac{v_{S0i}^2}{v_{P0i}^2}}\right). \qquad (A-11)$$

Substituting Eqs. (A-8)–(A-11) into Eq. (A-4) and taking the limit for the ray parameter $p\to 0$, we get Eq. (14).

A.2. Deriving Eq. (15) for c_2

When $k=1$,

$$c_2 = \frac{1}{6}\lim_{p\to 0}\frac{\mathrm{d}^3x_P}{\mathrm{d}x^3}.$$

By differentiating Eq. (A-5) with regard to p, after some tedious algebraic manipulation, one can get

$$\frac{\mathrm{d}^3x_P}{\mathrm{d}x^3} = \frac{\mathrm{d}}{\mathrm{d}p}\left(\frac{\mathrm{d}}{\mathrm{d}p}\left(\frac{\mathrm{d}x_P}{\mathrm{d}p}\frac{\mathrm{d}p}{\mathrm{d}x}\right)\frac{\mathrm{d}p}{\mathrm{d}x}\right)\frac{\mathrm{d}p}{\mathrm{d}x}$$
$$= \frac{(e_P+pf_P+e_S+pf_S)\left(3(e_Sg_P-e_Pg_S)+p\frac{\mathrm{d}}{\mathrm{d}p}(e_Sg_P-e_Pg_S)+\frac{\mathrm{d}}{\mathrm{d}p}(p^2(f_Sg_P-f_Pg_S))\right)}{(e_P+pf_P+e_S+pf_S)^5}$$
$$-\frac{3(2f_P+pg_P+2f_S+pg_S)(2(e_Sf_P-e_Pf_S)+p(e_Sg_P-e_Pg_S)+p^2(f_Sg_P-f_Pg_S))}{(e_P+pf_P+e_S+pf_S)^5} \qquad (A-12)$$

where

$$e=\sum_{i=0}^{n}U_i\Delta t_i,$$

$$f=\frac{\mathrm{d}e}{\mathrm{d}p}=\frac{\mathrm{d}}{\mathrm{d}p}\sum_{i=0}^{n}U_i\Delta t_i=\sum_{i=0}^{n}\frac{\mathrm{d}U_i}{\mathrm{d}p}\Delta t_i+p\sum_{i=0}^{n}U_i^2\Delta t_i,$$

and

$$g=\frac{\mathrm{d}f}{\mathrm{d}p}=\sum_{i=0}^{n}U_i^2\Delta t_i+\sum_{i=0}^{n}\frac{\mathrm{d}^2U_i}{\mathrm{d}p^2}\Delta t_i +3p\sum U_i\frac{\mathrm{d}U_i}{\mathrm{d}p}\Delta t_i+p^2\sum U_i^3\Delta t_i.$$

From Eqs. (A-8)–(A-11), by taking the limit of $p\to 0$, we get

$$\lim_{p\to 0}e_{\mathrm{P}}=\sum_{i=0}^{n}v_{\mathrm{P}2i}^2\Delta t_{\mathrm{P}0i}=V_{\mathrm{P}2}^2t_{\mathrm{P}0},\qquad(\mathrm{A}-13)$$

$$\lim_{p\to 0}e_{\mathrm{S}}=\sum_{i=0}^{n}v_{\mathrm{S}2i}^2\Delta t_{\mathrm{S}0i}=V_{\mathrm{S}2}^2t_{\mathrm{S}0},\qquad(\mathrm{A}-14)$$

$$\lim_{p\to 0}f_{\mathrm{P}}=\lim_{p\to 0}f_{\mathrm{S}}=0,\qquad(\mathrm{A}-15)$$

$$\lim_{p\to 0}g_{\mathrm{P}}=\lim_{p\to 0}\sum_{i=0}^{n}U_{\mathrm{P}i}^2\Delta t_{\mathrm{P}i}+\lim_{p\to 0}\sum_{i=0}^{n}\frac{\mathrm{d}^2U_{\mathrm{P}i}}{\mathrm{d}p^2}\Delta t_{\mathrm{P}i} =\sum_{i=0}^{n}v_{\mathrm{P}2i}^4\Delta t_{\mathrm{P}0i}+\sum_{i=0}^{n}8v_{\mathrm{P}0i}^4(\varepsilon_i-\delta_i) \times\left(1+\frac{2\delta_i}{1-\frac{v_{\mathrm{S}0i}^2}{v_{\mathrm{P}0i}^2}}\right)\Delta t_{\mathrm{P}0i},\qquad(\mathrm{A}-16)$$

and

$$\lim_{p\to 0}g_{\mathrm{S}}=\lim_{p\to 0}\sum_{i=0}^{n}U_{\mathrm{S}i}^2\Delta t_{\mathrm{S}i}+\lim_{p\to 0}\sum_{i=0}^{n}\frac{\mathrm{d}^2U_{\mathrm{S}i}}{\mathrm{d}p^2}\Delta t_{\mathrm{S}i} =\sum_{i=0}^{n}v_{\mathrm{S}2i}^4\Delta t_{\mathrm{S}0i}-\sum_{i=0}^{n}8v_{\mathrm{S}0i}^4\sigma_i \times\left(1+\frac{2\delta_i}{1-\frac{v_{\mathrm{S}0i}^2}{v_{\mathrm{P}0i}^2}}\right)\Delta t_{\mathrm{S}0i}.\qquad(\mathrm{A}-17)$$

Substituting Eqs. (A-13)–(A-17) into Eq. (A-12), the c_2 term of Taylor series expansion of conversion point in layered VTI media becomes

$$c_2=\frac{1}{6}\lim_{p\to 0}\frac{\mathrm{d}^3x_{\mathrm{P}}}{\mathrm{d}x^3}=\lim_{p\to 0}\frac{(e_{\mathrm{S}}g_{\mathrm{P}}-e_{\mathrm{P}}g_{\mathrm{S}})}{2(e_{\mathrm{P}}+e_{\mathrm{S}})^4} =\frac{1}{2}\frac{V_{\mathrm{S}2}^2t_{\mathrm{S}0}\sum_{i=0}^{n}\left(\Delta t_{\mathrm{P}0i}v_{\mathrm{P}0i}^4\left((1+2\delta_i)^2+8(\varepsilon_i-\delta_i)\left(1+\frac{2\delta_i}{1-\frac{v_{\mathrm{S}0i}^2}{v_{\mathrm{P}0i}^2}}\right)\right)\right)}{(V_{Pn2}^2t_{\mathrm{P}0}+V_{Sn2}^2t_{\mathrm{S}0})^4} -\frac{1}{2}\frac{-V_{\mathrm{P}2}^2t_{\mathrm{P}0}\sum_{i=0}^{n}\left(\Delta t_{\mathrm{S}0i}V_{\mathrm{S}0i}^4\left((1+2\sigma_i)^2-8\sigma_i\left(1+\frac{2\delta_i}{1-\frac{v_{\mathrm{S}0i}^2}{v_{\mathrm{P}0i}^2}}\right)\right)\right)}{(V_{\mathrm{P}2}^2t_{\mathrm{P}0}+V_{\mathrm{S}2}^2t_{\mathrm{S}0})^4}.\qquad(\mathrm{A}-18)$$

Eqs. (9) and (10) in combination with Eq. (A-18) gives Eq. (15).

Appendix B. Derivation of the C-wave moveout equations in layered VTI media

The *C*-wave reaction moveout equation for layered VTI has the form (Tsvankin and Thomsen, 1994):

$$t_{\mathrm{C}}^2=t_{\mathrm{C}0}^2+\frac{x^2}{V_{\mathrm{C}2}^2}+\frac{A_4x^4}{1+A_5x^2},\qquad(\mathrm{B}-1)$$

where

$$A_4=\frac{t_{\mathrm{C}0}V_{\mathrm{C}2}^4-\left(\sum_{i=1}^{n}(H_{\mathrm{P}i}+v_{\mathrm{P}2i}^4)\Delta t_{\mathrm{P}0i}+\sum_{i=0}^{n}(H_{\mathrm{S}i}+v_{\mathrm{S}2i}^4)\Delta t_{\mathrm{S}0i}\right)}{4t_{\mathrm{C}0}^3V_{\mathrm{C}2}^8},\qquad(\mathrm{B}-2)$$

$$H_{\mathrm{P}i}=8v_{\mathrm{P}0i}^4(\varepsilon_i-\delta_i)\left(1+\frac{2\delta_i}{1-1/\gamma_{0i}^2}\right),\qquad(\mathrm{B}-3)$$

and

$$H_{\mathrm{S}i}=-8v_{\mathrm{S}0i}^4\sigma_i\left(1+\frac{2\delta_i}{1-1/\gamma_{0i}^2}\right).\qquad(\mathrm{B}-4)$$

Using the parameters η_i and ζ_i defined by Eqs. (9) and (10), we obtain

$$H_{Pi} = 8v_{P2i}^4\eta_i, \qquad (B-5)$$

and

$$H_{Si} = -8v_{S2i}^4\zeta_i. \qquad (B-6)$$

Inserting the definitions of η_{eff} and ζ_{eff} from Eqs. (16) and (17) gives

$$\sum_{i=1}^{n}(H_{Pi} + v_{P2i}^4)\Delta t_{P0i} = (1 + 8\eta_{eff})t_{P0}V_{P2}^4, \qquad (B-7)$$

and

$$\sum_{i=1}^{n}(H_{Si} + v_{S2i}^4)\Delta t_{S0i} = (1 - 8\zeta_{eff})t_{S0}V_{S2}^4. \qquad (B-8)$$

Substituting Eqs. (B-7) and (B-8) into Eq. (B-2) gives

$$A_4 = \frac{t_{C0}V_{C2}^4 - ((1+8\eta_{eff})t_{P0}V_{P2}^4 + (1-8\zeta_{eff})t_{S0}V_{S2}^4)}{4t_{C0}^3V_{C2}^8}. \qquad (B-9)$$

Replacing V_{P2} and V_{S2} with V_{C2}, and t_{P0} and t_{S0} with t_{C0}, we obtain

$$A_4 = \frac{(\gamma_0\gamma_{eff} - 1)^2 + 8(1+\gamma_0)(\eta_{eff}\gamma_0\gamma_{eff}^2 - \zeta_{eff})}{4t_{C0}^2V_{C2}^4\gamma_0(1+\gamma_{eff})^2}. \qquad (B-10)$$

References

Alkhalifah, T., Tsvankin, I., 1995. Velocity analysis for transversely isotropic media. Geophysics 60, 1550–1566.

Bagaini, C., Bale, R., Caprioli, P., Ronen, S., 1999. Converted wave binning analysis: in search of γ. 69th Internat. Mtg., Soc. Explor. Geophys. Expanded., pp. 703–706.

Cheret, T., Bale, R., Leaney, S., 2000. Parameterization of polar anisotropic moveout for converted waves. 70th Annual Internat. Mtg., Soc. Expl. Expanded Abstracts., pp. 1181–1184.

Gaiser, J.E., Jackson, A.R., 2000. Accuracy and limitations of PS-wave converted-point computations: how effective is γ_{eff}? 70th Annual Internat. Mtg., Soc. Expl. Expanded Abstracts., pp. 1138–1141.

Grechka, V., Tsvankin, I., 1988. Feasibility of nonhyperbolic moveout inversion in transversely isotropic media. Geophysics 63, 957–969.

Li, X.-Y., Yuan, J., 1999. Converted-wave moveout and parameter estimation for transverse isotropy. 61st EAGE Conference, Expanded Abstract, vol. I, pp. 4–35.

Li, X.-Y., Yuan, J., 2001. Converted-wave imaging in inhomogeneous, anisotropic media: Part I. Parameter estimation. 63rd EAGE Conference, Expanded Abstract, vol. I, p. 109.

Tessmer, G., Behle, A., 1988. Common reaction point data-stacking technique for converted waves. Geophys. Prospect. 36, 671–688.

Thomsen, L., 1986. Weak elastic anisotropy. Geophysics 51, 1954–1966.

Thomsen, L., 1999. Converted-wave reflection seismology over inhomogeneous, anisotropic media. Geophysics 64, 678–690.

Tsvankin, I., 2001. Seismic Signatures and Analysis of Reaction Data in Anisotropic Media. Elsevier.

Tsvankin, I., Grechka, V., 2000a. Dip moveout of converted waves and parameter estimation in transversely isotropic media. Geophys. Prospect. 48, 257–292.

Tsvankin, I., Grechka, V., 2000b. Two approaches to anisotropic velocity analysis of converted waves. 70th Annual Internat. Mtg., Soc. Expl. Expanded Abstracts., pp. 1193–1196.

Tsvankin, I., Thomsen, L., 1994. Nonhyperbolic reflection moveout in anisotropic media. Geophysics 59, 1290–1304.

Yuan, J., 2002. Analysis of four-component seaoor seismic data for seismic anisotropy. PhD thesis, The University of Edinburgh.

Yuan, J., Li, X.-Y., 2002. C-wave anisotropic parameter estimation from conversion point. 64th EAGE Conference, Expanded Abstract, vol. II, p. 253.

Yuan, J., Li, X.-Y., Ziolkowski, A., Strijbos, F., 1998. Processing 4C sea-floor seismic data: a case example from the North Sea. 68th Ann. Internat. SEG Mtg., Expanded Abstracts., pp. 714–717.